ChemPubSoc Europe

DOI: 10.1002/slct.201602002

Chemistry SELECT Full Papers

Electro, Physical & Theoretical Chemistry

Electronic Properties and Ionic Photodissociation of Thionitrite Compounds RSNO [R = $(CH_3)_3C$– and $(CH_3)_2CH$–]

Antonela Cánneva,[a] Reinaldo L. Cavasso Filho,[b] Rosana M. Romano,[a] Carlos O. Della Védova,*[a] Shengrui Tong,[c] Maofa Ge,[c] and Mauricio F. Erben*[a]

The gas phase electronic properties of thionitrites (RSNO) in both the outermost (valence) and the shallow-core regions (S 2p) are experimentally studied for the first time by using photoelectron spectroscopy and synchrotron radiation in the VUV range with time-of-flight mass spectrometry in the Photoelectron Photoion Coincidence (PEPICO) mode. The He(I) photoelectron spectrum of *tert*-butyl thionitrite, $(CH_3)_3CSNO$, has been recorded and analyzed with the assistance of quantum chemical calculations. Furthermore, the dissociative photoionization mechanisms for two close related secondary and tertiary species, namely *iso*-propyl thionitrite, $(CH_3)_2HCSNO$ (**I**) and $(CH_3)_3CSNO$ (**II**), have been determined irradiating gaseous beams with photons in the 155–185 eV range, i.e. exciting and ionizing S 2p electrons of the central –SNO group. The branching ratio of ions produced on this way is analyzed allowing for a clear description of the main fragmentation channels operating after the electronic decay.

Introduction

Thionitrites (RSNOs) are important biological species involved in the transport and delivery of nitric oxide in blood plasma,[1,2] as well as signaling mechanisms,[3] mainly through the nitrosylation of cysteine residues of serum albumin and hemoglobin. Relevant review articles on biological aspects are available[4,5] covering the role of thionitrites on mammalian and plants.[6] Very recently, the physiological function of very simple species, such as perthionitrite[7] has been highlighted.[8,9]

Curiously, in spite of its biological relevance, physicochemical properties of thionitrites remain vastly unexplored, probably since most RSNOs are very unstable species. As early noted,[10] RSNOs are intense coloured species, which was interpreted as due to the presence of two absorption bands in the 500–600 nm range observed in the UV-Vis spectra, typically assigned to n→ π* transitions of the *syn* and *anti* conformers, respectively.[11] The gas-phase photodissociation of *tert*-butyl thionitrite $(CH_3)_3CSNO$ in the S_2 (n,π*) state was early studied by using two-photon LIF spectroscopy and the prompt dissociation via S–N bond cleavage was suggested.[12] More recently, Dick and co-workers used 3D-REMPI spectroscopy to demonstrate undoubtedly that both S_1 (π,π*) and S_2 (n,π*) are purely repulsive electronic states and the photolysis of $(CH_3)_3CSNO$ occurs *via* a direct fragmentation mechanism toward the formation of nitric oxide (NO) and the $(CH_3)_3CS$• radical.[13]

The photochemistry of thionitrites has also attracted much attention. Thus, CH_3SNO was observed as an intermediate in the OH-radical initiated oxidation of CH_3SCH_3 in the presence of NO, suggesting that the addition reaction of CH_3S• radical with NO takes place.[14] The gas-phase photodissociation of CH_3SNO irradiated with λ = 300–400 nm corroborated that the formed products are CH_3SSCH_3 and NO in stoichiometric amounts, suggesting that the S–N bond cleavage is a primary step.[15]

Protonated and deprotonated S-nitrosocysteine ions have been generated in the gas phase by electrospray ionization and studied by infra-red multiple photon dissociation (IRMPD) spectroscopy. The characteristic ν(NO) stretching vibration is clearly in the 1460–1490 cm^{-1} range in the IRMPD spectrum of deprotonated species, providing a signature for the S-nitrosation process.[16] Most recently, ions of the S-nitroso derivative of L-glutathione were generated in the gas phase and the conformational properties determined by interpreting the infra-red spectra.[17]

Sulphur K-edge X-ray absorption spectroscopy (XAS) was applied for two S-nitroso proteins in the solid phase, namely N-acetyloxy-3-nitrosothiovaline (SNAP) and N-(N–L-γ-glutamyl-S-nitroso-L-cysteinyl)-glycine (GSNO).[18] The electronic structure of RSNOs was revealed by analyzing the XAS pre-edge features, especially the sulphur 3p character of the unoccupied orbitals.

[a] *Dr. A. Cánneva, Prof. Dr. R. M. Romano, Prof. Dr. Dr. C. O. Della Védova, Prof. Dr. M. F. Erben*
CEQUINOR (UNLP-CONICET, CCT, La Plata)
Departamento de Química
Facultad de Ciencias Exactas
Universidad Nacional de La Plata
Bv. 120 Nro. 1465, La Plata (CP 1900)
República Argentina
Tel.: + 54-221-445-4393
E-mail: erben@quimica.unlp.edu.ar
carlosdv@quimica.unlp.edu.ar

[b] *Prof. Dr. R. L. C. Filho*
Universidade Federal do ABC
Av. dos Estados, 5001, CEP 09210-580 Santo André, São Paulo, Brazil

[c] *Dr. S. Tong, Prof. Dr. M. Ge*
State Key Laboratory for Structural Chemistry of Unstable and Stable Species
Beijing National Laboratory for Molecular Sciences (BNLMS)
Institute of Chemistry
Chinese Academy of Sciences
Beijing 100190, People's Republic of China

Supporting information for this article is available on the WWW under http://dx.doi.org/10.1002/slct.201602002

For the GSNO species, the main transitions from the S 1 s toward unoccupied π*(SNO), σ*(N–S) and σ*(S–C) orbitals appear at 2471.4, 2473.3 and 2474.9 eV, respectively, while for SNAP the corresponding values are 2471.3, 2472.9 and 2474.2 eV, respectively. The possibility of using this spectroscopic technique as an analytical tool for the determination of the in vivo concentration of RSNOs has been suggested.[18] Recent studies were performed also by using S K-edge XAS including trityl thionitrite, $(C_6H_5)_3CSNO$.[19] Moreover, simulated sulphur K-edge spectra were computed for "model" RSNO compounds [R = CH_3, C_2H_5, $CH(CH_3)_2$ and $C(CH_3)_3$], suggesting that other factors than electronic effects should play a key role determining the reactivity of thionitrites.

Here, we report for the first time gas phase photoionization study on thionitrite species irradiated in the VUV and soft X-ray regimes by using synchrotron-based PEPICO time-of-flight mass spectrometry. Two close related substances that are relatively stable liquids at room temperature with enough vapor pressure have been selected: the secondary *iso*-propyl thionitrite $(CH_3)_2CHSNO$ (**I**) and the tertiary *tert*-butyl thionitrite, $(CH_3)_3CSNO$ (**II**).[20] Furthermore, the He(I) photoelectron spectrum of $(CH_3)_3CSNO$ is reported.

Results and Discussion

Photoelectron Spectra and photoionization in the Outermost Valence region

Although the valence electronic distribution of nitrites compounds, RONO, are vastly studied,[21–23] experimental reports on PE spectra for thionitrites could not be found in the literature. Now the He(I) PE spectrum of $(CH_3)_3CSNO$ is depicted in Figure 1, and the experimental and theoretical ionization

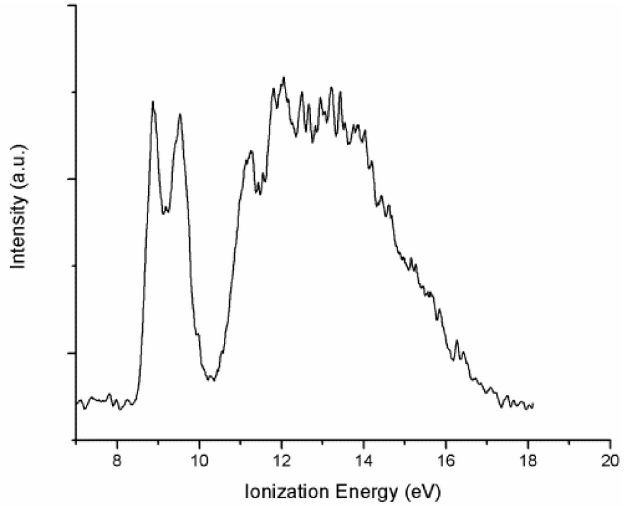

Figure 1. He(I) photoelectron spectrum of $(CH_3)_3CSNO$.

energies are listed in Table 1. The geometry of both *syn* and *anti* conformers of $(CH_3)_3CSNO$ in the ground electronic state

Table 1. Experimental and Calculated Ionization Energies (OVGF/6-311 + G (2df)) (eV) and MO Characters for $(CH_3)_3CSNO$

IE_{exp}(eV)	*anti*[a] [b]	*syn*[a] [b]	Assignment	Symmetry
8.91	8.95 (0.88)	8.97 (0.88)	n_π(S)	a"
9.60	9.40 (0.89)	9.52 (0.89)	n(O)	a′
11.33	11.19 (0.90)	11.05 (0.90)	π(N=O)	a"
11.95	12.19 (0.91)	12.33 (0.91)	σ(C–H)s	a′, a" [c]
12.45	12.23 (0.91)	12.32 (0.91)	n(N)	a′
12.93	13.35 (0.91)	13.43 (0.91)	σ (C–S)	a′
13.21	14.01 (0.91)	14.01 (0.91)	π (S–N)	a"

[a] Values calculated at the OVGF/6-311 + G(2df) level of approximation with B3P86/6-311 + G(2df) optimized geometries. [b] Values in parenthesis correspond to pole strength. [c] This experimental value corresponds to nine orbitals of the type σ(C–H) with both a′ and a″ symmetry according calculations.

belongs to the C_S symmetry point group.[24] Thus, the canonical molecular orbitals of type a′ are typically σ-orbitals lying in the symmetry plane, while those of type a" are π-orbitals. The assignments of PE spectrum bands to photoionization processes from specific molecular orbital were made with reference to the results from the OVGF/6-311 + G(2df) calculations [geometry optimization at the B3P86/6-311 + G(2df) level of approximation]. Similar ionization values are computed for these conformers and the characters determined for the molecular orbitals are the same at the level of theory used in this work (see Table 1). The characters of the highest occupied molecular orbital of the most stable *anti* conformer are shown in Figure 2.

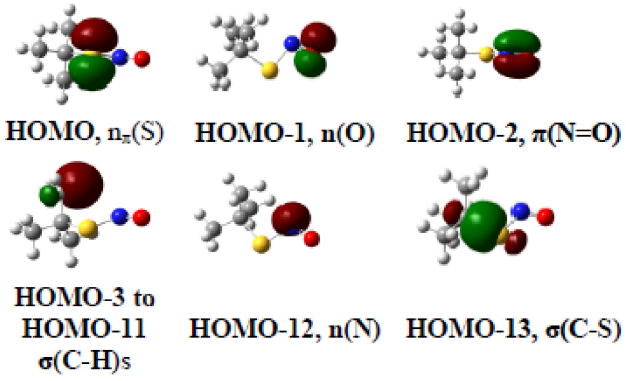

Figure 2. Characters of the highest occupied orbitals of *anti* $(CH_3)_3CSNO$.

The outermost electronic distribution reveals that the highest occupied orbitals are associated with the thionitrite group. Thus, HOMO with a" symmetry can be observed as an orbital nominally localized on the sulphur atom occupied by lone-pair electrons. Its vertical ionization potential value is reasonably low, 8.91 eV, as compared with the oxygen analogue (10.12 eV).[25] The following two bands in the PE spectrum at 9.60 and 11.33 eV were assigned to be originated from the nO (a′) and π (N=O) (a″), respectively. This assignment

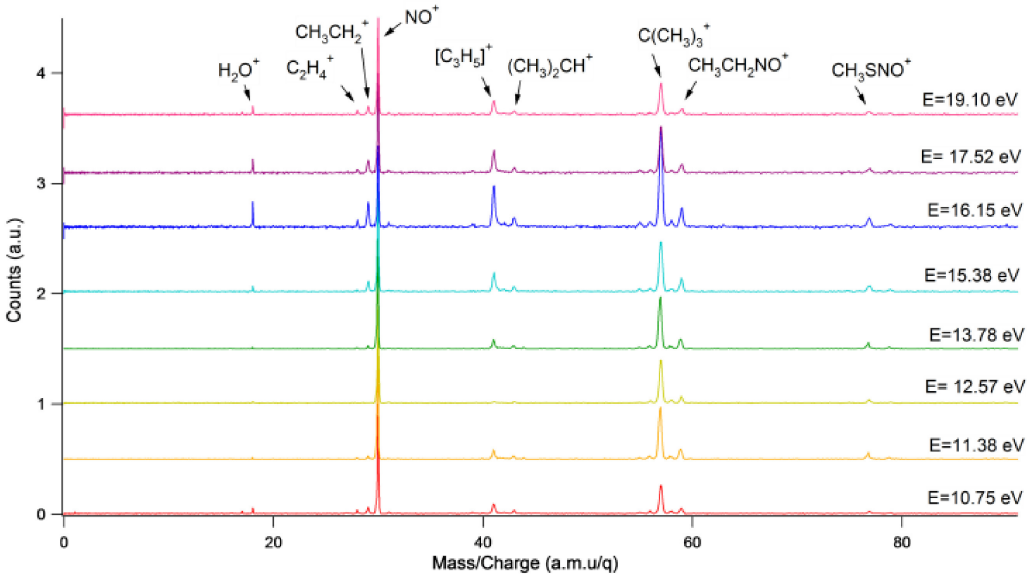

Figure 3. PEPICO spectra of $(CH_3)_3$ CSNO at selected irradiation energies.

Table 2. Branching Ratios (%) for Selected Fragment Ions Extracted from PEPICO Spectra Taken at Selected Photon Energies in the Valence Region of $(CH_3)_3$ CSNO.

m/z (amu/q)	Ion	Photon Energy (eV) 10.75	11.38	12.57	13.78	15.38	16.15	17.52
29	$CH_3CH_2^+$	4.2	1.6	-	2.8	6.3	6.7	7.8
30	NO^+	37.3	38.8	44.8	30.5	28.6	10.9	18.1
41	$[C_3H_5]^+$	7.8	5.7	3.3	9.7	10.9	13.2	11.5
42	$C(CH_3)_2^+$	-	-	-	-	3.4	4.7	4.6
43	$CH(CH_3)_2^+$	2.5	2.0	2.5	4.4	4.0	6.6	4.5
55	$[C_4H_7]^+$	2.3	1.1	-	1.3	2.7	4.3	5.5
56	$C(CH_2)(CH_3)_2^+$	2.3	2.1	3.1	3.0	3.5	4.4	4.1
57	$(CH_3)_3C^+$	17.8	31.7	31.5	22.6	22.8	19.9	16.7
59	$CH_3CH_2NO^+$	4.0	5.9	5.4	7.2	6.9	7.3	5.7
77	CH_3SNO^+	2.7	3.3	3.9	5.7	5.0	5.2	6.8
79	$(CH_3)_2SOH^+$	2.3	1.1	2.1	4.0	3.1	4.7	3.8

is well supported by the OVGF/6-311 + G(2df) calculations, with computed values of 8.95 eV (HOMO), 9.40 and 11.19 eV, respectively. These are the most reliable data obtained from the PES spectrum.

The TOF-mass spectra in the PEPICO mode for $(CH_3)_3CSNO$ irradiated at selected energies in the valence region are shown in the Figure 3 and branching ratios for ion production are given in Table 2. When photons with 10.75 eV are used very simple spectra are obtained, with intense signals at m/z = 30 (NO^+) and 57 [*tert*-butyl cation, $(CH_3)_3C^+$].

From the analysis of the PEPICO spectra, it becomes apparent that the main photoionization channels opened after ionization of valence electrons lead to the formation of NO^+ (m/z = 30) and $(CH_3)_3C^+$ (m/z = 57), together with minor amounts of alkyl cations. Thus, the ruptures of the S–N and C–S bonds are primary dissociation steps after the ionization of valence electrons. Typical inductive fragmentations can be supposed, as shown in Scheme 1.

The analysis of the PEPICO spectra reveals that rearrangement reactions are likely to occur in this photon energy range. It is worth noticing the observation of signals at m/z = 29, 59 and 79, that can be assigned to the alkyl $CH_3CH_2^+$ and $CH_3CH_2NO^+$ ions, and to the rather unusual $(CH_3)_2SOH^+$ sulphenic acid cation,[26] respectively.

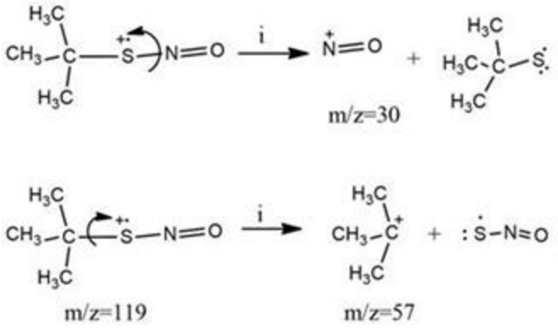

Scheme 1. Inductive fragmentation mechanisms for the formation of m/z = 30 and 57 cations.

Total Ion Yield Spectra and photoionization in the S 2p Inner–shell region.

The Total Ion Yield spectra for thionitrites **I** and **II** in the S 2p edge are shown in Figure 4. The potential ionizations occur at

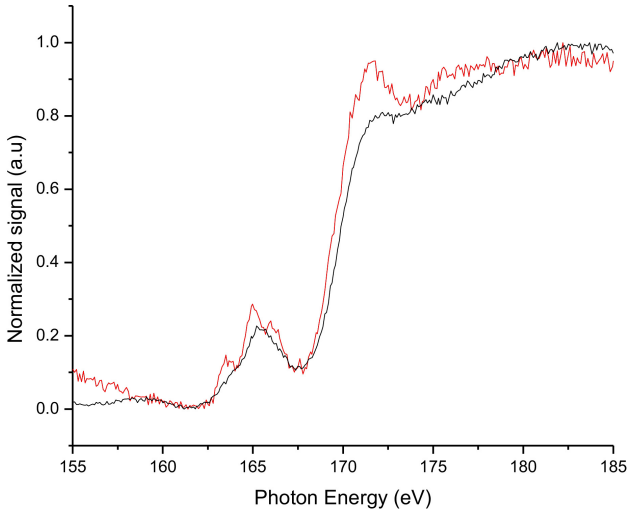

Figure 4. TIY spectra of $(CH_3)_2CHSNO$ (red line) and $(CH_3)_3CSNO$ (black line) in the photon energy range 155.0 – 185.0 eV.

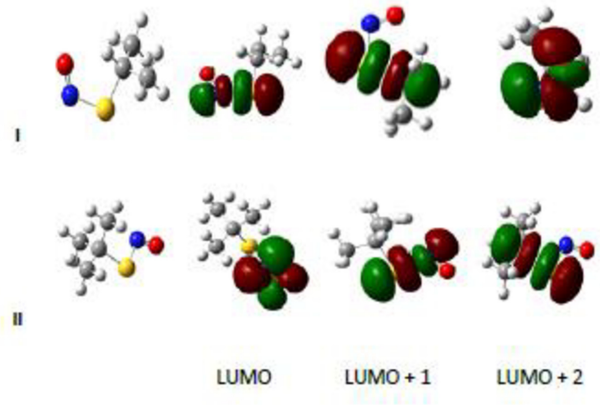

Figure 5. Computed lowest vacant valence molecular orbitals of compounds **I** and **II.**.

171.9 and 171.6 eV, respectively and clear pre-edge features can be observed at 163.5, 165.0 and 166.0 eV for **I** and at 164.1 and 165.3 eV for **II.** Significant sulfur 3p character have been recognized for the lowest vacant orbitals of thionitrites mainly associated with the –SNO group.[13] Since the bound state transitions from the core sulfur levels are mostly localized on the sulfur atom, sulfur K- and L-edges based spectroscopic techniques are expected to be highly specific for the determination of chemical speciation for thionitrites, including detailed information on the electronic structure of the –SNO group. In the present case, the tentative assignment of these electronic transitions toward vacant orbitals has been performed based on the experimental UV spectra as well as assisted by quantum chemical calculations. In the case of $(CH_3)_2CHSNO$, the 163.5 eV peak is associated with the S 2p→ LUMO transition, corresponding to a final state with a strong σ*(S–N) character, whereas two signals at 165.0 and 166.0 eV are well-resolved and assigned to the σ*(S–C) and π*(NO) transitions, respectively.

The low intensity signal observed in the TIY spectra of compound **II** at 164.1 eV is due to S 2p→ LUMO transition, mainly associated with the excitation to the π*(NO) antibonding orbital. The following broad and more intense resonance band observed at 165.3 eV can be originated by resonant transitions populating the σ*(N–S) and σ*(S–C) vacant orbitals. The small intensity of the lowest lying resonance compared with the 165.3 eV band reflects the degree of π character in the S 2p→ LUMO transition.

As noted by Kennepohl and coworker,[19] it is expected that S 2p→ π*(NO) and S 2p→ σ*(N–S) excitation energies of RSNO's decrease with increasing the electron donation capacities of R, the larger effect being observed when primary thionitrites are considered. In our case, the extension of this behavior toward tertiary species is also valid, provided that R is electron donating as the *tert*-butyl group. The change in the order of the virtual orbitals between **I** and **II**, mostly explained by the stabilization of the π*(NO) for compound **II**, can be also analyzed by examining their UV-Vis spectra.[24] In effect, the HOMO→ LUMO transitions for **I** and **II** occur at 550 and 590 nm, respectively in the experimental spectra, in qualitative agreement with our TIY spectra.

Different electron decay mechanisms –and ionic dissociations- take place depending on whether the primary photon absorption conducts to a core-hole excitation or ionization processes. The ion production after the core-hole electronic decay of **I** and **II** were measured at resonant and threshold excitation energies of S 2p electrons, as well as at photon energy corresponding to the S 2p ionization. Figures 6 and 7 show the PEPICO spectra measured at 165.0 and 165.3 eV for **I** and **II**, respectively. The complete fragment assignment with their relative abundances is presented in Table 3.

It is interesting to notice that the parent ion, M^+, is observed as low abundant but clearly defined signals in both spectra of compounds **I** (105 m/z) and **II** (119 m/z). The well-known sensitivity of thionitrites toward UV-Vis irradiation is not in contradiction with the observation of the parent ion peak. In the present case and using energies of about 165 eV the final ionized ionic state can be comparatively more stable than the electronically excited species. In particular, the photon-energy tunability of synchrotron radiation allows promoting the occurrence of participant Auger process at resonant transitions by emitting a valence electron, such as the non-bonding electrons as the HOMO and HOMO-1 on the S or O atoms, respectively. Thus, the one-hole final state corresponding to the M^+ cations is stable against dissociation, because the bond orders are the same as those in the parent molecules. Thus, it can be assumed that cationic states populated after the S 2p inner shell excitation are relatively bonded and M^+ of both **I**

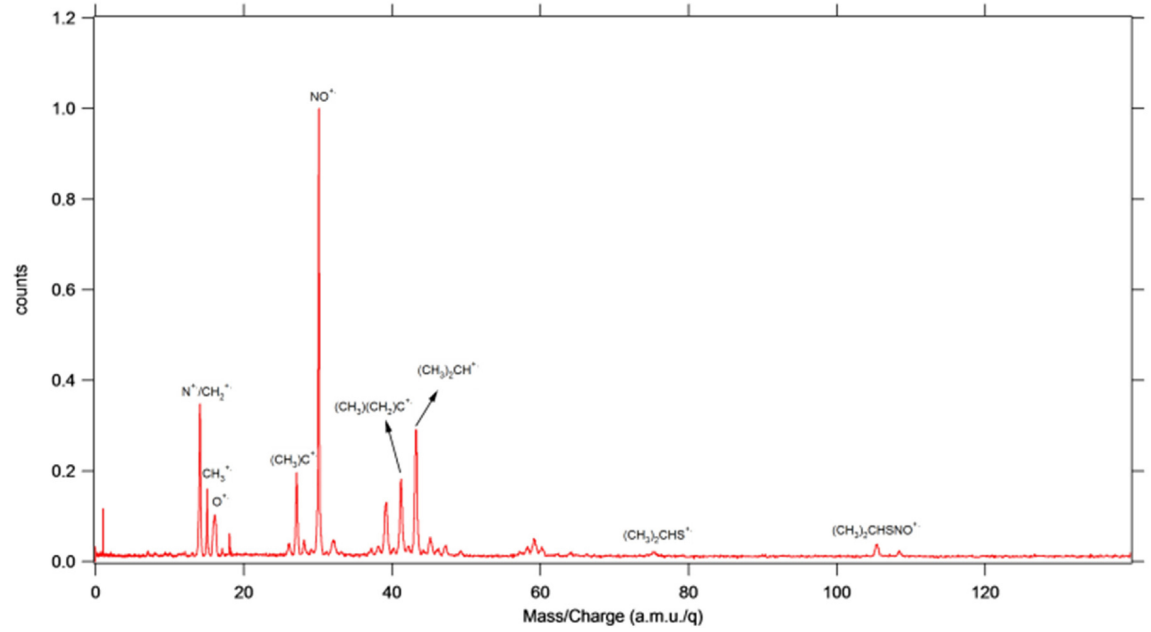

Figure 6. Normalized PEPICO spectrum of $(CH_3)_2CHSNO$ measured at 165.0 eV.

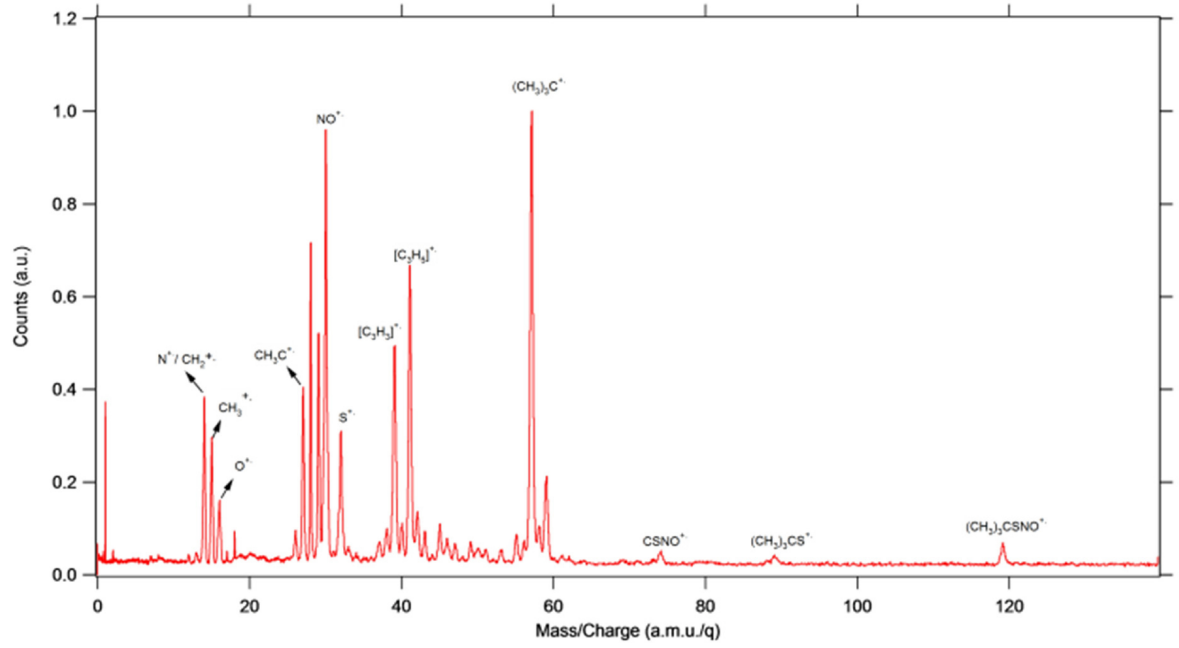

Figure 7. Normalized PEPICO spectrum of $(CH_3)_3CSNO$ measured at 165.3 eV.

and **II** are stable in the microsecond time scale of the present experiments.

Dissociative cationic states that conduct to the fragmentation of the species are also simultaneously reached, leading to the formation of molecular and atomic cations. One of the most important ions produced in the photoionization of both compounds here studied corresponds to NO^+, amounting 17.3 and 12.9% for **I** and **II** irradiated at 164.9 and 165.0 eV, respectively. It can be observed that the peaks at m/z 30 are well-resolved (especially for compound **I**) with the typical narrow shape associated with ionization processes that release low kinetic energies. Thus, it is possible that the simply charged $M^{\bullet+}$ parent ion directly dissociates forming NO^+ and the corresponding RS• radicals, via a direct two-body dissociation mechanisms. On the other hand, it should be noted that when S 2p excitation energies are reached, the $[M–NO]^+$ cations are

Table 3. Branching Ratios (%) for Fragment Ions Extracted from PEPICO Spectra Taken at a Photon Energy around S 2p Energies for $(CH_3)_2CHSNO$ (I) and $(CH_3)_3CSNO$ (II).

m/z	Fragment	Photon Energy (eV) 150.0		153.0	155.0	163.5	164.9	165.0	166.2	171.0	171.7	172.0	181.0	
		I	II	I	II	I	I	II	I	II	I	II	I	II
1	H^+	2.5	3.2	2.1	3.4	3.1	2.2	3.2	2.5	2.1	3.4	2.6	3.4	2.9
12	C^+	-	-	-	1.1	0.9	-	1.2	-	1.4	1.1	1.2	0.9	1.1
14	CH_2^+/N^+	14.7	19.0	16.9	8.6	14.2	10.6	6.3	10.5	5.9	7.2	10.3	8.3	3.5
15	CH_3^+	5.0	6.2	3.8	4.8	3.8	3.6	4.8	3.6	7.7	4.3	4.1	4.5	6.1
16	O^+	7.9	9.0	8.8	4.3	7.9	6.0	3.6	6.0	1.6	4.2	5.7	4.6	2.2
27	$(CH_2)CH^+/CH_3C^+$	4.1	3.1	3.5	4.2	4.1	5.3	5.0	5.6	5.6	6.0	5.0	6.5	4.5
30	NO^+	-	25.5	24.5	12.0	20.9	17.3	12.9	17.5	3.4	16.4	19.6	17.5	17.2
32	S^+	2.0	-	1.8	3.8	2.1	2.6	5.3	3.1	5.8	3.1	2.7	3.5	5.3
39	$[C_3H_3]^+$	4.5	5.8	3.3	6.2	4.0	4.9	7.7	5.4	8.3	5.0	4.8	5.8	6.7
41	$[C_3H_5]^+$	5.0	5.2	3.9	8.2	4.6	5.8	8.6	5.8	9.1	5.9	5.3	5.9	6.5
42	$(CH_3)_2C^+/CH_3CHCH_2^+$	-	1.2	0.7	1.3	1.0	1.4	2.2	1.3	-	-	0.8	-	1.4
43	$CH(CH_3)_2^+$	5.8	2.1	4.2	1.9	5.3	7.9	-	7.3	1.7	7.1	6.0	6.9	-
57	$(CH_3)_3C^+$	-	7.0	-	10.2	-	-	11.6	-	12.0	-	1.0	-	7.1
74	$CSNO^+$	-	-	-	0.9	-	-	1.1	-	2.6	-	-	-	1.5
75	$(CH_3)_2CHS^+$	-	-	-	-	1.4	1.2	-	1.1	-	1.1	-	1.4	-
89	$(CH_3)_3CS^+$	-	-	-	0.6	-	-	1.0	-	2.4	-	-	-	1.2
105	$(CH_3)_2CHSNO^+$	2.6	-	1.8	-	1.4	1.4	-	1.4	-	0.8	-	0.7	-
119	$(CH_3)_3CSNO^+$	-	-	-	1.2	-	-	1.4	-	1.7	-	-	-	0.6

observed as weak signals at m/z = 75 and 89 for **I** and **II**, respectively. The detection of these heavy fragments in the PEPICO spectra implies that they are originated from the corresponding single charged parent ions, formed through resonance Auger decay processes. Thus, the rupture of the S-N bond is a primary process in the ionic dissociation of **I** and **II**, as shown in Scheme 2:

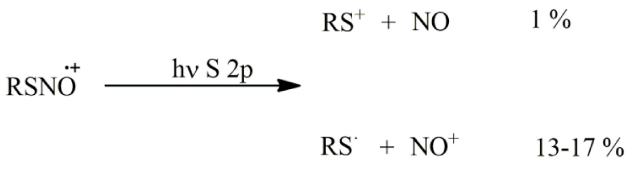

Scheme 2. RS–NO bond rupture in the dissociative ionization of thionitrites after S 2p excitation.

The PEPICO spectra for compound **I** show the presence of another intense signal at m/z = 43, corresponding to $(CH_3)_2CH^+$ fragment, i.e. the $[M–SCO]^+$ ion, reaching 7.9% abundance at the 164.9 eV resonance transition. The analogous loss of the SNO fragment for compound **II** lead to the formation of the m/z = 57 ion, with a relative intensity of 11.6% at the main resonance transition (165.0 eV). Dissociation processes on S 2p excited RSNO species, lead to the formation of *iso*-propyl and *tert*-butyl carbocations, R^+, with apparently higher stability for the tertiary species. This finding is in line with the well-known alkyl-carbocation stability trend (tertiary > secondary > primary) and the higher stabilization through donation of the electrons in σ(C–H) bonds to the empty p orbital of the carbocation, i.e. hyperconjugation.

Many other alkyl cations derived from the R groups of **I** (i.e. *iso*-propyl) and **II** (i.e. *tert*-butyl) are observed in the PEPICO spectra, as listed in Table 3.

Conclusions

The first photoelectron spectrum of a thionitrite species in the gas phase was measured and interpreted with the help of electron propagator calculations at the OVGF/6-311 + G(2df) level of approximation. The electronic structure in the valence region of $(CH_3)_3CSNO$ is characterized by ionizations of electrons formally located at the thionitrite moiety. Thus, low energy bands observed in the spectrum at 8.91, 9.60, and 11.33 eV are associated with ionization processes from the outermost n_π(S) (HOMO), n(O) and π(N=O) orbitals, respectively. After ionization with photons in the VUV region (10.7-17.5 eV), the NO^+ (m/z = 30) and $(CH_3)_3C^+$ (m/z = 57) cations are the most abundant ions detected in the PEPICO mass spectra.

Synchrotron-based studies were extended also toward the inner-shell region by using 155–185 eV photons. The total ion yield spectra shown a series of pre-edge features associated with excitations to vacant orbitals with antibonding characters. The S 2p→ LUMO transitions are observed at 164.1 and 163.5 eV, while the S 2p ionization edges occur at 171.9 and 171.6 for **I** and **II**, respectively. The S 2p absorption spectra is explained in terms of different LUMO orbitals, namely σ*(S–N) and π*(NO), for **I** and **II**, respectively.

Gas phase photoionization after inner-shell excitation at the S 2p level has been determined for $(CH_3)_2CHSNO$ and $(CH_3)_3CSNO$ species by recording the PEPICO spectra at selected photon energies. It is worth to mention that both parent ions and the base peaks corresponding to the NO^+ ion were observed in the mass spectra of **I** and **II**, with small contributions of the corresponding RS^+ cations. Photofragmen-

tation processes leading to the formation of R^+ ions are also important routes in the ionic dissociation of RSNOs. The nature of the R group clearly influence the extent of this dissociation channel, the formation of tertiary carbocations, like $(CH_3)_3C^+$ in **II**, being favored over secondary ones, as $(CH_3)_2CH^+$ in **I.**

These results demonstrate that dominant fragmentation channels for ionized RSNO species, -in both the valence and inner-shell regions-, involve the dissociation of the S–N and R–S bonds, with a relevant role played by the R substituent in final fate of S 2p excited RSNO, i.e. in the photoion branching ratio.

Acknowledgements

This work has been largely supported by the Brazilian Synchrotron Light Source (LNLS) under Proposals TGM-1449 and TGM-8887. The authors wish to thank Prof. Dr. Arnaldo Naves de Brito and his research group for fruitful discussions and generous collaboration during their several stays in Campinas and the TGM beamline staffs for their assistance throughout the experiments. They are also indebted to the Agencia Nacional de Promoción Científica y Tecnológica (ANPCyT, PICT 2130 and PICT 2957), Consejo Nacional de Investigaciones Científicas y Técnicas (CONICET) PIP 348 and 352, and the Facultad de Ciencias Exactas, Universidad Nacional de La Plata for financial support.

Conflict of Interest

The authors declare no conflict of interest.

Keywords: electronic properties · electronic structure · S-nitrosothiols · synchrotron radiation · photodissociation

[1] L. Jia, C. Bonaventura, J. Bonaventura, J. S. Stamler, *Nature.* **1996**, *380*, 221–226.
[2] J. S. Stamler, D. I. Simon, J. A. Osborne, M. E. Mullins, O. Jaraki, T. Michel, D. J. Singel, J. Loscalzo, *Proc. Natl. Acad. Sci.* **1992**, *89*, 444–448.
[3] A. Martínez-Ruiz, I. S. M. Araújo, A. Izquierdo-Álvarez, P. Hernansanz-Agustín, S. Lamas, J. M. Serrador, *Antioxid. Redox Signal.* **2013**, *19*, 1220–1235.
[4] J. S. Stamler, E. J. Toone, *Curr. Opinion Chem. Biol.* **2002**, *6*, 779–785.
[5] D. D. Thomas, D. Jourd'heuil, *Antioxid. Redox Signal.* **2012**, *17*, 934–936.
[6] O. Lamotte, J. B. Bertoldo, A. Besson-Bard, C. Rosnoblet, S. Aimé, S. Hichami, H. Terenzi, D. Wendehenne, *Front. Chem.* **2015**, *2*, 1–10.
[7] R. Wedmann, A. Zahl, T. E. Shubina, M. Dürr, F. W. Heinemann, B. E. C. Bugenhagen, P. Burger, I. Ivanovic-Burmazovic, M. R. Filipovic, *Inorg. Chem.* **2015**, *54*, 9367–9380.
[8] M. M. Cortese-Krott, B. O. Fernandez, M. Kelm, A. R. Butler, M. Feelisch, *Nitric Oxide.* **2015**, *46*, 14–24.
[9] M. M. Cortese-Krott, A. R. Butler, J. D. Woollins, M. Feelisch, *Dalton Trans.* **2016**, *45*, 5908–5919.
[10] S. Oae, Y. H. Kim, D. Fukushima, K. Shinhama, *J. Chem. Soc. Perkin Trans. 1.* **1978**, 913–917.
[11] S. Oae, K. Shinhama, K. Fujimori, Y. H. Kim, *Bull. Chem. Soc. Jpn.* **1980**, *53*, 775–784.
[12] M. R. S. McCoustra, J. Pfab, *Chem. Phys. Lett.* **1987**, *137*, 355–360.
[13] A. Schmaunz, U. Kensy, A. Slenczka, B. Dick, *J. Phys. Chem. A.* **2010**, *114*, 9948–9962.
[14] R. P. Steer, B. L. Kalra, A. R. Knight, *J. Phys. Chem.* **1967**, *71*, 783–784.
[15] H. Niki, P. D. Maker, C. M. Savage, L. P. Breitenbach, *J. Phys. Chem.* **1983**, *87*, 7–9.
[16] F. Lanucara, B. Chiavarino, M. E. Crestoni, D. Scuderi, R. K. Sinha, P. Maître, S. Fornarini, *Int. J. Mass Spectrom.* **2012**, *330–332*, 160–167.
[17] B. Gregori, L. Guidoni, B. Chiavarino, D. Scuderi, E. Nicol, G. Frison, S. Fornarini, M. E. Crestoni, *J. Phys. Chem. B.* **2014**, *118*, 12371–12382.
[18] R. K. Szilagyi, D. E. Schwab, *Biochem. Biophys. Res. Comm.* **2005**, *330*, 60–64.
[19] V. Martin-Diaconescu, I. Perepichka, D. S. Bohle, P. Kennepohl, *Can. J. Chem.* **2011**, *89*, 93–97.
[20] A. M. Wenge, A. Schmaunz, U. Kensy, B. Dick, *Phys. Chem. Chem. Phys.* **2012**, *14*, 7076–7089.
[21] E. Matyus, G. Magyarfalvi, G. Tarczay, *J. Phys. Chem. A.* **2007**, *111*, 450–459.
[22] W. Dianxun, L. Sheng, L. Ying, Z. Shijun, D. Chuanfan, G. Yiqin, C. Wenwu, *J. Electron Spectrosc. Rel. Phenom.* **1996**, *82*, 19–22.
[23] X. Zeng, L. Yao, W. Wang, F. Liu, Q. Sun, M. Ge, Z. Sun, J. Zhang, D. Wang, *Spectrochim. Acta A.* **2006**, *64*, 949–955.
[24] A. Cánneva, M. F. Erben, R. M. Romano, Y. V. Vishnevskiy, C. G. Reuter, N. W. Mitzel, C. O. Della Védova, *Chemistry - Eur. J.* **2015**, *21*, 10436–10442.
[25] Z. Sun, S. J. Zheng, D. X. Wang, *Acta Chim. Sin.* **2001**, *59*, 2031–2033.
[26] F. Turecek, D. E. Drinkwater, F. W. McLafferty, *J. Am. Chem. Soc.* **1989**, *111*, 7696–7701.

Submitted: December 19, 2016
Revised: February 8, 2017
Accepted: February 8, 2017